One-dimensional combined field and thermionic emission model and comparison with experimental results

Xin He, John Scharer,[a] John Booske, and Sean Sengele
Electrical and Computer Engineering Department, University of Wisconsin-Madison, Madison, Wisconsin 53706

(Received 4 September 2007; accepted 28 January 2008; published 1 April 2008)

An integrated theoretical model has been developed to predict the entire range of emission from thermionic to field emission, including the mixed emission regime. The model assumes a Sommerfeld free electron model supply function, for which the Fermi-Dirac distribution applies with a nonzero temperature. The electron transmission coefficient is calculated in one dimension using a transfer matrix method (TMM) to solve the steady-state Schrödinger equation. Emission current densities have been measured for a periodic copper knife-edge cathode to compare with the TMM model result. It is shown that the computational result utilizing this model provides good agreement with the experimental data. Unambiguous and reliable estimates of the effective field enhancement factor β_{eff} ($\beta_{\text{eff}}=E_s/E_g$, where E_s is the cathode surface electric field and E_g is the gap electric field between the cathode and anode) and the effective work function ϕ_{eff} are obtained from experimental measurements using this model by simultaneously fitting thermionic and field emission data for the cathode. Comparing the experimental and theoretical results reveals that finite temperature thermal contributions to the current emission can be significant in the operation of many field emission cathodes. © *2008 American Vacuum Society.* [DOI: 10.1116/1.2884755]

I. INTRODUCTION

The processes of field and thermionic emissions are described via the Fowler-Nordheim (FN) and Richardson-Laue-Dushman (RLD) laws,[1–4] respectively. The supply electrons obey the Sommerfeld free electron model[5] for which the Fermi-Dirac distribution applies. The transmission coefficient is obtained via the solution of the one dimensional time independent Schrödinger equation.

In Fig. 1, the potential barrier with an electron image force is given as[3]

$$V(Z) = -W_a \quad \text{for } Z < 0, \tag{1}$$

$$V(Z) = -eE_sZ - \frac{e^2}{16\pi\varepsilon_0 Z} \quad \text{for } Z > 0, \tag{2}$$

where e is the elementary positive charge and E_s is the cathode surface electric field. The Z direction is normal to the metal-vacuum surface. The Z component of energy is W_Z and W_a is the common electric potential inside the metal. ζ is the Fermi level for the metal. Here, $-e^2/16\pi\varepsilon_0 Z$ represents the image potential energy.

The supply function $N(W_Z,E)$, (where E is the total electron energy) which follows the Sommerfeld free electron model and the Fermi-Dirac distribution is given as[5]

$$N(W_Z,E)dW_Z dE = \frac{4\pi m}{h^3}\frac{dW_Z dE}{\exp((E-\zeta)/kT)+1}, \tag{3}$$

where m is the mass of the electron, h is Planck's constant, k is the Boltzmann constant, and T is the background temperature.

In the original FN law,[1] the image charge potential was not included and a simple triangular potential barrier was applied. In this case, assuming that all electron energies are below the top of the potential energy barrier, the transmission coefficient $D(W_Z)$ can be analytically solved by the modified Airy function approach.[6] Considering the full charge image potential barrier, a JWKB (Ref. 7) approximation method was applied to obtain an analytical solution. The transmission coefficient is solved as[6]

$$D(W_z) \cong \exp\left(-c + \frac{W_z-\zeta}{d}\right), \tag{4}$$

where

$$c = \frac{4\sqrt{(2m\phi^3)}}{3\hbar eE_s}v(y),$$

$$d = \frac{\hbar eE_s}{2\sqrt{2m\phi}t(y)},$$

and

$$y = \sqrt{(e^3E_s)/4\pi\varepsilon_0}/\phi,$$

where $v(y)$ and $t(y)$ are well-known special field emission elliptic functions due to image charge potential, ϕ is the work function, and E_s is the surface electric field. Reference 8 provides a simple approximate solution for v, t, and y.

[a]Author to whom correspondence should be addressed; electronic mail: scharer@engr.wisc.edu

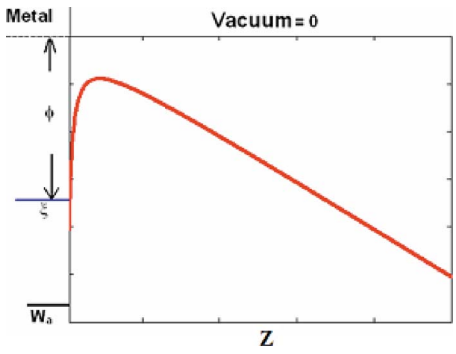

FIG. 1. Potential barrier between the metal and vacuum interfaces.

Note that Eq. (4) is an approximate result that only applies for $W_Z \ll V_{\max}$ (the maximum energy of the potential barrier) and for the emission range $W \sim \zeta$.

After integrating the product of the supply function and transmission coefficient, the standard FN equation for the local current density J is obtained as

$$J = e\int_{-\infty}^{\infty}\int_{E}^{-W_a} D(W_z)N(W_z,E)dW_s dE$$
$$= \frac{e^3E_S^2}{8\pi h\phi t^2(y)}\exp\left[-\frac{4\sqrt{(2m)}\phi^{3/2}}{3\hbar eE_S}\upsilon(y)\right]\frac{\pi kT/d}{\sin(\pi kT/d)}$$
$$= \frac{A_{\mathrm{FN}}E_s^2}{\phi t^2(y)}\exp\left(-\frac{B\phi^{3/2}\upsilon(y)}{E_s}\right)\frac{\pi kT/d}{\sin(\pi kT/d)}. \quad (5)$$

For the standard FN equation, we let $T=0$ and obtain

$$J = \frac{A_{\mathrm{FN}}E_s^2}{\phi t^2(y)}\exp\left(-\frac{B\phi^{3/2}\upsilon(y)}{E_s}\right). \quad (6)$$

For the RLD law,[9] the transmission coefficient is simply defined as 1 for $W_z > V_{\max}$ and 0 for $W_z < V_{\max}$. This approximation is applicable for very low electric fields and high temperatures. In the standard RLD law, E_s is set to 0. The standard RLD equation is written as

$$J(E_s,T,\phi) = A_R T^2\exp(-\phi/KT), \quad (7a)$$

where the proportionality constant A_R, known as Richardson's constant, is given by

$$A_{\mathrm{R}} = 4\pi emk^2/h^3. \quad (7b)$$

The FN equation is widely used in field emission cathode characterization. In experiments, usually only the applied voltage, the anode-cathode gap distance, the macroscopic cathode area A_{cathode}, and the emission current can be measured directly. Other cathode parameters, such as the work function ϕ, the effective field enhancement factor for the most strongly emitting surface sites $\beta_{\mathrm{eff}}=E_s/E_g$, (where E_g is the mean field between the electrodes), and the the effective emitting area A_{emit} or the emission area ratio, $R_{\mathrm{area}}=A_{\mathrm{emit}}/A_{\mathrm{cathode}}$, needs to be extracted from the experimental results indirectly.

β_{eff} parameters are often obtained by fitting measured I-V data to the standard FN equation using a so-called FN plot. On writing $J=I/A_{\mathrm{emit}}=I/(R_{\mathrm{area}}A_{\mathrm{cathode}})$ and putting Eq. (6) into so-called FN coordinates, we obtain

$$\ln\left(\frac{I}{E_g^2}\right) = \ln\left(\frac{R_{\mathrm{area}}A_{\mathrm{cathode}}A_{\mathrm{FN}}\beta_{\mathrm{eff}}^2}{t^2(y)\phi}\right) - \frac{\upsilon(y)B\phi^{3/2}}{\beta_{\mathrm{eff}}E_g}. \quad (8)$$

On defining

$$X \equiv \frac{1}{E_g},$$

$$Y \equiv \ln\left(\frac{\mathrm{I}}{E_g^2}\right), \quad (9)$$

we obtain

$$Y = \ln\left(\frac{R_{\mathrm{area}}A_{\mathrm{cathode}}A_{\mathrm{FN}}\beta_{\mathrm{eff}}^2}{t^2(y)\phi}\right) - \frac{\upsilon(y)B\phi^{3/2}}{\beta_{\mathrm{eff}}}X. \quad (10)$$

It is well known that over the range of fields where the standard FN equation is valid as an approximate description of the electron emission, this theoretical plot of Y against X is expected to be a nearly straight line.

We can convert the experimental values of voltage V to E_g using the formula $E_g=V/d_g$, where d_g is the anode-cathode separation, and hence obtain experimental values of X and Y. The fitting procedure normally used is equivalent to fitting these values by an equation that represents the tangent to Eq. (10) and contains slope and intercept correction factors[10] rather than $\upsilon(y)$ and $t^{-2}(y)$. However, what one then obtains from the fitted slope is an estimate of $B\phi^{3/2}/\beta_{\mathrm{eff}}$. In the conventional approach, the parameters β_{eff} and ϕ are linked together in a complex, nonseparable manner. As is evident from Eqs. (10) and (11), the quality of the fit to experimental data is sensitively influenced by the combination of choices for these two parameters, leaving it ambiguous as to what the "true" (*in situ*) values of these parameters are for any particular experiment. Usually, a precise, independent measurement of ϕ or β_{eff} is not available. Interestingly, applications utilizing this or an equivalent curve-fitting method to extract an estimate for β_{eff} often reports a very high β_{eff} and unreasonably low values of R_{area}. The likely reasons for this will be shown later in this article. However, a more accurate yet convenient method is needed for unambiguous and accurate cathode parameter extraction that also allows for additional effects, such as the influence of a nonzero temperature. Given the need to include nonzero temperature effects (the case for which is made in this article), we developed a new method for improved cathode parameter extraction.

Previous research[6,11–15] on the transition through mixed emission (ME) between the two limiting regimes of pure field emission (FE) and pure thermionic emission (TE) has been conducted. These references provide models and expressions that expand the range of validity of the RLD and FN equations to provide a more general emission theory. Many papers utilize approximate methods to obtain a general equation for FE, TE, and the transition process between

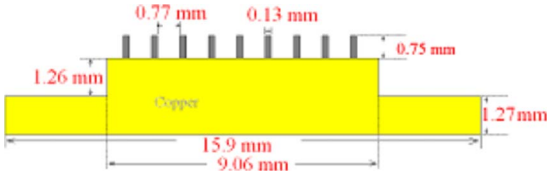

FIG. 2. Sketch of the CKE cathode.

them. In this article, by calculating the transmission coefficient $[D(W_Z)]$ via the transfer matrix method[16] (TMM) model directly and substituting $D(W_Z)$ into Eq. (5) for numerical integration, a prediction of the entire range of emission from thermionic to field emission including mixed emission is achieved which is not limited, for example, by the JWKB approximation assumption.

II. EXPERIMENTAL SETUP AND CATHODE STRUCTURE

The measurements are conducted in the Madison cathode experiment facility which consists of two parts, an ultrahigh vacuum chamber and electrical measurement components. The vacuum part of the facility consists of a six-way-cross stainless steel chamber, a scroll pump, a turbopump, and a vacuum-ion pump. Operation is designed for UHV vacuum (10^{-10} Torr) with bake-out provisions up to temperatures of 450 °C for several days to eliminate any residual water vapor or other contaminants. Three pumps are used to achieve UHV vacuum. The first is a scroll pump, working from atmospheric pressure to 10^{-3} Torr. Then, a turbomolecular pump is used to reduce the pressure from 10^{-3} to 10^{-8} Torr. Finally, a vacuum-ion pump brings the whole system to 10^{-10} Torr after 450 °C baking.

A high-voltage dc supply and a high-voltage switch provide 0–20 kV, 1 μs–5000 ms duration negative pulses with rise times less than 60 ns. The pulsed voltage is applied between the cathode and anode to obtain the current-voltage characteristics. A vacuum feedthrough linear translator is used to adjust the cathode-anode gap from 0 to 2.5 cm with a resolution of 50 μm. To reduce electromagnetic pickup noise, all voltage supplies are well shielded by an aluminum box so that currents down to 5 nA can be measured. Moreover, all connectors and cables are coaxial with careful attention paid to ensure excellent shielding and electrical grounding. To measure the lowest currents, a three-stage cascaded amplifier with accessory filtering and a current limiting circuit was designed and employed to measure the emission current levels down to 5 nA.

Emission current has been measured for a periodic copper knife-edge (CKE) cathode at elevated temperatures. The knife-edge features (0.13 mm wide and 0.75 mm high) are fabricated on a copper substrate using wire-electric discharge machining. The structure of this cathode is shown in Fig. 2.

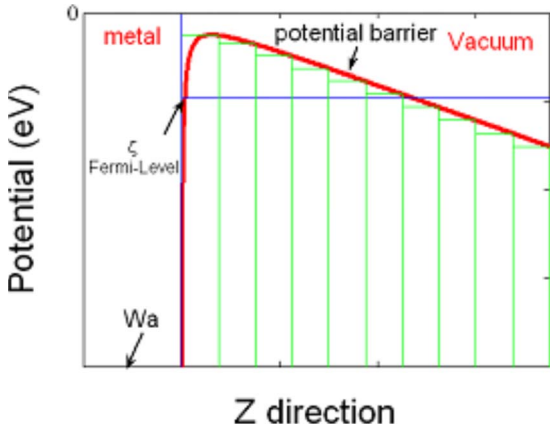

FIG. 3. Potential barrier between the metal-vacuum surface and narrow rectangular segments used in the TMM model.

III. TMM MODEL SIMULATION FOR EMISSION CURRENT DENSITY

To predict the emission current for the whole range from TE to FE including mixed emission (ME), a TMM model is developed. The model assumes a Sommerfeld free electron model supply function, for which the Fermi-Dirac distribution applies with a nonzero temperature. The energy barrier between the metal and vacuum surfaces includes the full image charge force potential term rather than triangular barrier approximations. Electron tunneling is calculated directly in one dimension using a TMM model to solve the steady-state Schrödinger equation without the JWKB approximation.

In the TMM (Ref. 16) model, the spatially varying potential barrier at the metal-vacuum interface is divided into many narrow rectangles, as shown in Fig. 3. The number of the rectangles needs to be high enough to allow the simulation to converge, which depends on the surface electric field applied. Typically, lower electric fields need more rectangles since the potential barrier is thicker.

Figure 4 illustrates a benchmark for our TMM code model result at 330 °C and for an idealized triangular barrier (neglecting the image charge potential contribution). This problem provides an opportunity to compare the TMM results with the original FN model which is solved exactly for this case with an Airy function directly at $T=0$ K and utilizing the RLD equations that are relevant for lower values of E_s.

For high electric fields, the TMM model result with a simplified triangular potential barrier assumption overlaps with the original FN equation result precisely, which utilizes a triangular potential barrier without consideration of the image charge potential. When the image charge potential is incorporated, the TMM model's predicted current density is larger than that of the original FN equation result since the image charge force potential will reduce the potential barrier height. At low electric fields, the TMM model's predicted current density levels come close to but slightly less than that of the RLD law.[7] The reason for the small difference is that the RLD law uses a simplified estimation for the transmission coefficient. The RLD law transmission coefficient for

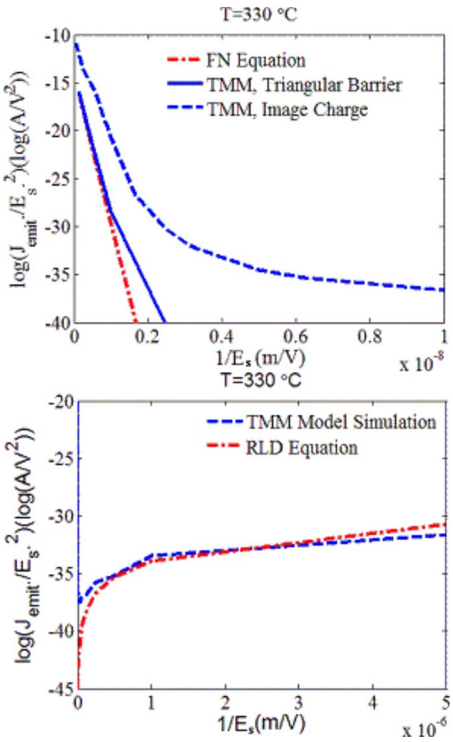

FIG. 4. Benchmarking against conventional analytic solutions: (a) TMM with triangular potential barrier (solid) and image charge potential (dashed) compared to conventional FN equation (dot dash); (b) TMM compared with the Richardson-Laue-Dushman equation for low surface electric fields.

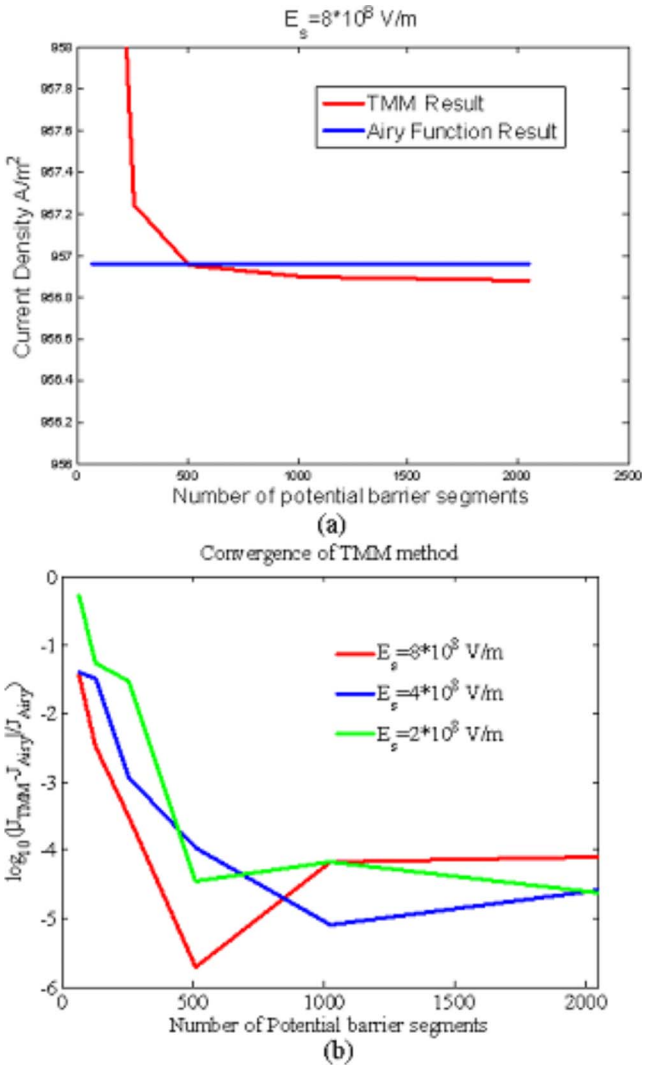

FIG. 5. TMM model convergence and accuracy.

electrons having a kinetic energy higher than the potential barrier is assumed to be 1 and the transmission coefficient for electrons having a kinetic energy lower than the potential barrier is assumed to be 0. Considering quantum mechanical principles, the electron transmission coefficient can be lower than 1 even if the electron's energy level is higher than the potential barrier because of the prospect of reflection. The regime with medium electric field between FN law and RLD law is named as the ME regime. A minimum of $\ln(J/E_s^2)$ occurs in the ME regime when the emission transfers from FE to TE, which has been widely observed in the experiments by our and other groups.[17–22]

We now examine the convergence of the TMM model with respect to the number of elements for different values of the surface electric field E_s. To compare the final accuracy of the TMM model result with the analytical solution (Airy function solution[23]), a pure triangular potential barrier is applied, meaning that the image charge potential is not included.

Figure 5 shows the convergence property of the TMM model referenced to the analytical solution of an Airy function. It is shown that with the increase of the number of segments, the emission current density approaches the Airy function solution rapidly. When the number of segments is higher than 500, the difference between the TMM solution and Airy function is less than 1×10^{-4}, which is adequate for most experimental applications. This discrepancy could be due to the fact that a finite number of segments is used, numerical precision errors, or the precision of the Airy function's numerical evaluation. However, since the purpose of our TMM model simulation is to interpret the experimental data, this accuracy is sufficient.

We have also compared the predictions of the TMM model to the widely used Murphy-Good equations in Figs. 6(a)–6(c). Figure 6(a) shows the emission current density estimated from a cathode with an illustrative work function of 4.5 eV (typical for copper, graphite, and other pure materials) at a temperature of 330 °C. At high electric fields (or small $1/E_g$), the predicted emission current density from the TMM model (now including the image potential contribution) is in excellent agreement with the Murphy-Good prediction for the field emission regime. At very low electric fields (or high $1/E_g$), the predicted emission current density from the TMM model is again in excellent agreement with the Murphy-Good prediction for the thermionic emission regime. However, for medium range electric fields, the Murphy-Good mixed emission equation set does not necessarily predict the emission accurately over the region span-

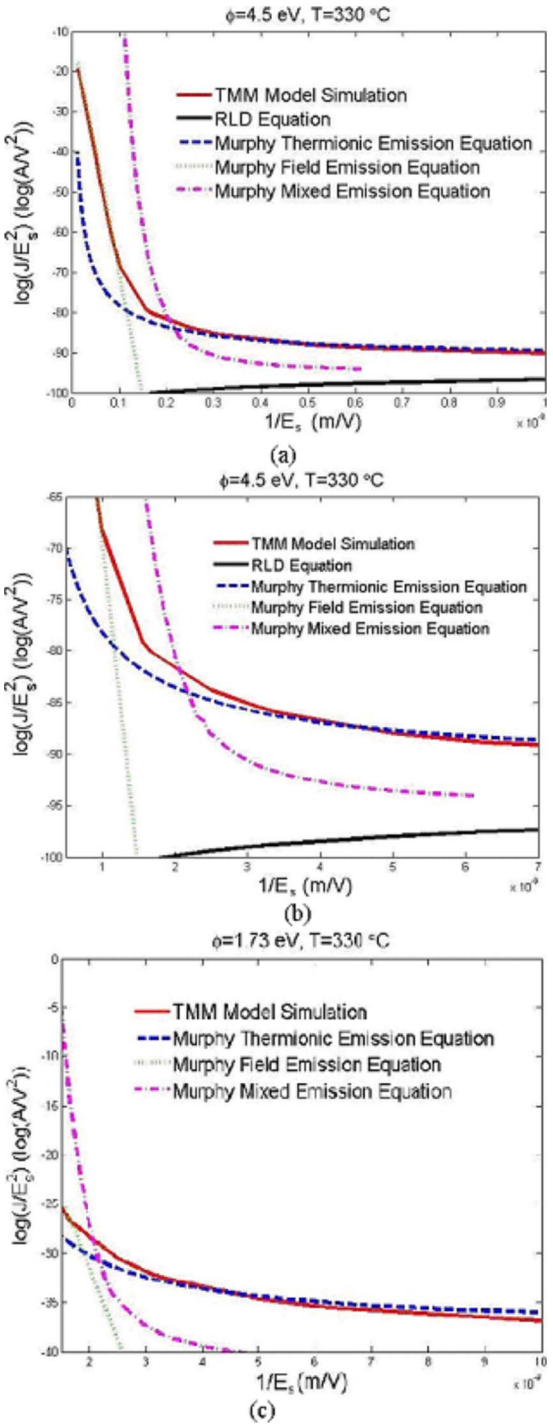

FIG. 6. TMM model comparison with Murphy's equations.

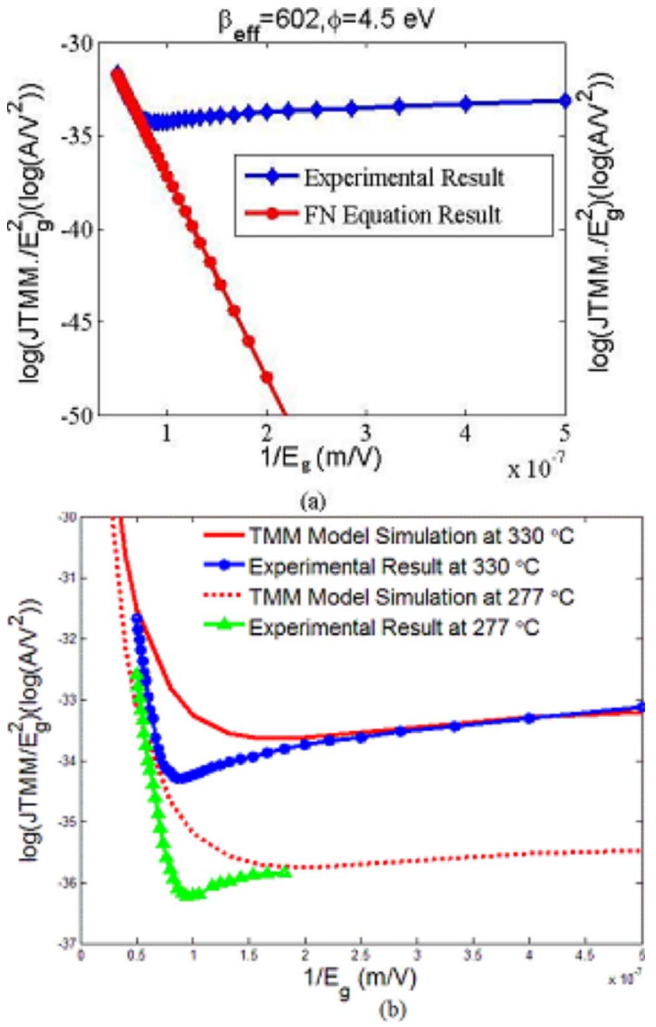

FIG. 7. Fitting with the (a) FN equation and (b) TMM model at 330 and 277 °C.

ning the field emission and thermionic emission regimes. Figure 6(b) [which is an enlarged view of Fig. 6(a)] starkly illustrates that the mixed emission equation of the Murphy-Good set only predicts the emission accurately for a very narrow electric field region, at least for this illustrative set of parameters. It does not provide a smooth transition between the field emission and thermionic emission regimes. This is consistent with the results of Ref. 12 (refer to Fig. 6 of Ref. 12). Meanwhile, Fig. 6(c) shows the same comparison with a work function equal to 1.7 eV, which corresponds to the effective work function for our CKE cathode, extracted from our experimental data. In this case, the Murphy-Good mixed emission equation provides better agreement since the region where the emission current density is not accurately predicted is smaller. This is because the gap between the Fermi level and the apex peak of the potential barrier is smaller for lower work functions. This reduces the size of the region over which the approximations applied in the Murphy-Good equations do not agree with the experimental results.

IV. RESULTS AND DISCUSSION

Figure 7 shows a detailed comparison of the experimental and TMM modeling results. In many papers, only the linear high electric field region is fitted with the FN equation and the low electric field part (lower than the minimum point electric field) is ignored and attributed to noise or leakage current since the cathode is regarded as "off" below this electric field. As illustrated below, this approach may intro-

duce substantial ambiguity and inaccuracies. When only the linear high electric field region is fitted with the FN equation, either ϕ or β_{eff} needs to be known *a priori* or assumed in order to determine the other value. However, it is quite often the case that both of them are not well known since their direct measurements are very hard to accomplish, especially *in situ*. A popular method is to assume a ϕ obtained from the measured work function of the pure metal, even though oxidation and impurity atom adsorption can occur even in excellent vacuum conditions and can change ϕ significantly (an *in situ* effect that is not easily characterized by *ex situ* measurements of ϕ). To illustrate the challenge, we first apply the conventional parameter extraction approach by fitting the high electric field subset of our data to the standard FN equation. The fitting result is shown in Fig. 7(a) assuming the work function of pure copper, 4.5 eV. The result obtained implies a correspondingly large field enhancement factor, $\beta_{\text{eff}} \sim 600$. This is much higher than predicted from electrostatic simulations of the ridge shape of the cathode without any surface microstructure using the FEM code MAXWELL 2D.[24] Those simulations predict a much lower β_{eff} value of approximately 4. A corresponding extremely small emission area ratio of $R_{\text{area}} \sim 10^{-11}$ is obtained. Using the ridge top area of 9×10^{-6} m^2 as A_{cathode}, this implies a nonphysically large emission current density of 1.4×10^8 A/cm^2 and an emission area of about 10^{-16} m^2, implying that only 2000–3000 atoms participate in the entire emission process. This is physically suspect.

In contrast, Fig. 7(b) illustrates a comparison of our experimental results with the TMM predictions for two different temperatures. Both the high electric field data and low electric field data are fitted consistently with our model. The portion of the data for low electric fields is carefully analyzed to confirm that it is not due to noise. In the low electric field region, the slope of the $\ln(J/E_g^2)$ curve is nearly independent of β_{eff}. Therefore, we adjust only the ϕ_{eff} parameter in our TMM computational model to fit the thermal right-hand portion of the $\ln(J/E_g^2)$ vs $1/E_g$ curve. By assuming an effective emitting area ratio, $R_{\text{area}}=1$, we fitted the theoretical prediction to the data to obtain a particular value for the effective work function ϕ_{eff}. For our cathode, the effective work functions extracted for 330 and 277 °C are 1.73 and 1.69 eV, respectively. The difference of 0.04 eV is reasonable explained by the slight change between experiments in surface condition as impurity adsorbate coverage. The extracted effective work function is low but plausible. Postexperiment examination of our CKE cathode revealed surface discoloration likely due to either oxidation or carbon atom adsorption. Several recent publications[25,26] report an effective work function for oxidized copper surfaces lower than 2.8 eV, similar to our low extracted value. Although the work function of bulk pure CuO is much higher,[27] it is expected that the surface work function for oxidized copper could be substantially reduced by dipole inducing[28] impurity adsorbates on the cathode surface. Microstructures could also reduce the work function. Substituting the obtained values of $\phi_{\text{eff}}=1.69$ and 1.73 eV into our TMM computational model, we fitted to the experimental results in the high electric field regime and obtain in both cases a good fit with $\beta_{\text{eff}}=8$. This is comparable with the estimate we have obtained from macroscopic finite-element electrostatic simulations. β_{eff} is varied by 10% to provide a somewhat better fitting result.

TABLE I. Work function variation with R.

Work function Φ (eV)	Emission area ratio R_{area}
1.73	1
1.72	0.8
1.69	0.5
1.65	0.2
1.61	0.1
1.49	0.01

We assumed $R_{\text{area}}=1$ for both the low-field and high-field fittings, i.e., $A_{\text{emit}}=A_{\text{cathode}}$, where A_{cathode} was taken to be the area of the top of the ridges, as noted earlier. In practice, we find that ϕ_{eff} and β_{eff} are only weakly dependent on R_{area}. As shown in Table I, when R_{area} is reduced from 100% to 1%, ϕ_{eff} only varies from approximately 1.7 to 1.5 eV (14%). The corresponding β_{eff} does not change with variations in R. This justifies our assumption of $R_{\text{area}}=1$ for extracting estimates for the effective experimental values of ϕ and β_{eff}.

To clarify why there is such a large difference between conventional FN fitting and TMM model fitting, we examined whether our experimental conditions lie in FE, TE, or ME regimes. Different definitions have been put forth for FE, TE, and ME regimes. The early equations and definitions were provided by Murphy and Good.[17] Recently, Jensen *et al.* have made further progress.[2,14] Here, we provide a complementary way to identify the FE, TE, and ME regimes. For a general emission current density $J_{E,T}$ at a given surface electric field E_s and temperature T, we define $J_{E,0}$ as the pure field emission current density with the surface electric field equal to E_s and a temperature of 0 K. Similarly, $J_{0,T}$ is the emission current density with a surface electric field equal to 0 V/m and a nonzero temperature T. $J_{E,0}/J_{E,T}$ and $J_{0,T}/J_{E,T}$ are plotted in Fig. 8 assuming illustrative values of $\phi=1.73$ eV and $T=330$ °C. There are three distinct regions in the figure. For low surface electric fields, $J_{0,T}/J_{E,T} \sim 1$ and $J_{E,0}/J_{E,T} \sim 0$, i.e., the electric field effects are negligible. For high surface electric fields, the opposite is true with temperature effects being negligible. Between these two regions, both electric field and temperature effects are important. We identify the ME regime to be that where the emitted current differs from either pure FE or pure TE by more than 10%. Comparing the results of Fig. 7 to the data in Fig. 8, we see that for $\beta_{\text{eff}}=8$, the entire range of the experimental data represents mixed emission, neihter solely FE nor fully TE, and therefore the FN equation is not accurate in this regime. In this regime, both temperature and field effects play an important role in the resulting emission current. This is especially remarkable since Fig. 7(a) demonstrates that the high electric field data can be visually fitted to the FN equation with apparent good agreement. Without our TMM

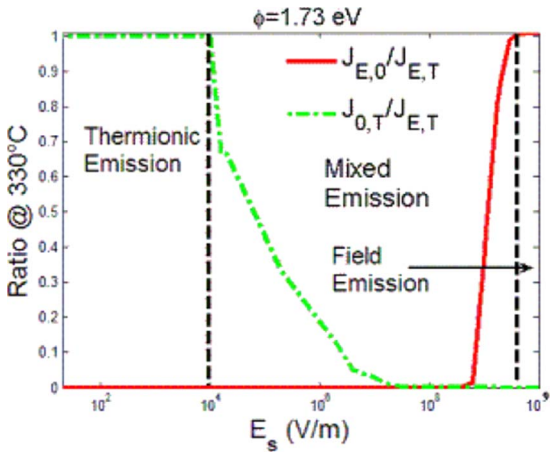

FIG. 8. FE, TE, and ME regimes.

model analysis, one would likely underestimate the importance of thermal emission contributions to the "field emission" current and inappropriately apply the FN equation to evaluate the cathode under test.

Even at quite high electric fields, the FN equation may not be a correct description if the temperature (local or global) is sufficiently high. This is because the minimum electric field required for the FE regime is a function of temperature. As shown in Fig. 9 (ϕ=1.73 eV), when the temperature increases, the minimum electric field required to be in the FE regime also increases. This observation may also apply to other FE cathode experiments. Many FE cathodes are designed to achieve very large surface electric fields by the use of large-aspect-ratio, field-enhancing emitter tips. This means that the cathode conduction current flows through small cross-sectional area emitters, and for steady or near-continuous operation, the temperatures of the emitting tips can be very high due to locally intense Ohmic heating.

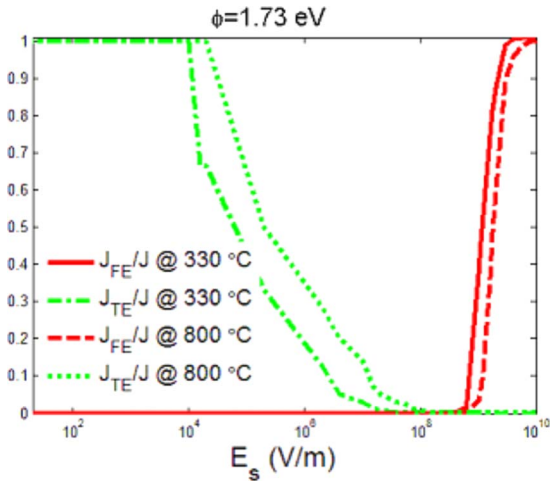

FIG. 9. FE, TE, and ME regime variation with temperature.

V. CONCLUSION

In summary, a TMM model has been developed to provide a straightforward calculation for the entire range of cathode emission from thermionic to field emission, including mixed emission. This model's prediction can provide good agreement with the experimental data and provides reasonable values for the cathode's average effective field enhancement factor and work function. This research shows that what might typically be assumed to be a pure Fowler-Nordheim field emission current regime can include very significant nonzero temperature contributions. Using a combined thermal/field emission model is important for cathode modeling and extraction of cathode parameters, particularly for materials with low work functions. Future work will examine possible variations in the R_{area} and β_{eff} values that could vary with applied electric field to provide further improvements in the comparison of the TMM with the experimental results.

ACKNOWLEDGMENTS

This research was supported through AFOSR by a US-DOD MURI05 grant on the Nano-physics of High Current Density Cathode and Breakdown.

[1]L. W. Nordheim and L. W. Nordheim, Proc. R. Soc. London, Ser. A **119**, 173 (1928).
[2]Kevin L. Jensen, J. Appl. Phys. **102**, 024911 (2007).
[3]G. Furse, *Field Emission in Vacuum Microelectronics* (Kluwer Academic Dordrecht, Plenum, New York, 2005).
[4]A. Sommerfeld and H. Bethe, Handbuch der physic **24**, 442 (1933).
[5]R. D. Young, Phys. Rev. **113**, 110 (1959).
[6]Kevin L. Jensen, J. Vac. Sci. Technol. B **21**, 1528 (2003).
[7]H. Froman and P. O. Froman, *JWKB Approximation-Contribution to the Theory* (North-Holland, Amsterdam, 1965).
[8]R. G. Forbes, Appl. Phys. Lett. **89**, 113122 (2006).
[9]O. W. Richardson, *The Emission of Electricity from Hot Bodies* (Longmans, Green, New York, 1921).
[10]R. G. Forbes, J. Vac. Sci. Technol. B **17**, 526 (1999).
[11]S. C. Miller and R. H. Good, Phys. Rev. **91**, 174 (1953).
[12]E. L. Murphy and R. H. Good, Phys. Rev. **102**, 1464 (1956).
[13]W. W. Dolan and W. P. Dyke, Phys. Rev. **95**, 327 (1954).
[14]Kevin L. Jensen and Marc Cahay, Appl. Phys. Lett. **88**, 154105 (2006).
[15]Kevin L. Jensen, Patrick G. O'Shea, and Donald W. Feldman, Appl. Phys. Lett. **81**, 3867 (2002).
[16]Mohsen Razavy, *Quantum Theory of Tunneling* (World Scientific, Singapore, 2003).
[17]Y. W. Zhu, T. Yu, F. C. Cheong, X. J. Xu, C. T. Lim, V. B. C. Tan, J. T. L. Thong, and C. H. Sow, Nanotechnology **88**, 16 (2005).
[18]Reui-San Chen, Ying-Sheng Huang, Ya-Min Liang, Chim-Sung Hsieh, Dah-Shyang Tsai, and Kwong-Kau Tiong, Appl. Phys. Lett. **84**, 1552 (2004).
[19]Yo-Sep Min, Eun Ju Bae, Jong Bong Park, Un Jeong Kim, Wanjun Park, Jaewon Song, Cheol Seong Hwang, and Noejung Park, Appl. Phys. Lett. **90**, 263104 (2007).
[20]Baoqing Zeng, Guangyong Xiong, Shuo Chen, Wenzhong Wang, D. Z. Wang, and Z. F. Ren, Appl. Phys. Lett. **90**, 033112 (2007).
[21]Byeongchul Ha and Cheol Jin Lee, Appl. Phys. Lett. **90**, 023108 (2007).
[22]Masahiro Miyauchi, Hiromasa Tokudome, Yoshitake Toda, Toshio Kamiya, and Hideo Hosono, Appl. Phys. Lett. **89**, 043114 (2006).
[23]T. Choy, A. Harker, and A. Stoneham, J. Phys.: Condens. Matter **16**, 861

(2004).
[24]Ansoft Corporation (http://www.ansoft.com).
[25]C. T. Hsieh, J. M. Chen, H. H. Lin, and H. C. Shih, Appl. Phys. Lett. **83**, 3383 (2003).
[26]Y. W. Zhu, T. Yu, F. C. Cheong, X. J. Xu, C. T. Lim, V. B. C. Tan, J. T. L. Thong, and C. H. Sow, Nanotechnology **16**, 88 (2005).
[27]F. P. Koffyberg and F. A. Benko, J. Appl. Phys. **53**, 1173 (1982).
[28]Vasilios Vlahos, John H. Booske, and Dane Morgan, Appl. Phys. Lett. **91**, 144102 (2007).